Dirac Points in Two-Dimensional Semi-Metal B_5ScNi Monolayer with Low Symmetry

Wen-Juan Li[1,2] · Na Li[3] · Bao-Min Zhang[3] · Wei-Xiao Ji[3]

Abstract

Two-dimensional (2D) Dirac semi-metal (DSM) materials have been studied in depth for their excellent transmission properties and potential applications in nanoscale electronic devices, while DSMs with low symmetric configuration still lack research on them. In this work, we propose a 2D DSM, namely a B_5ScNi monolayer, which has a structure with only one mirror symmetry, using first-principles calculations based on density functional theory. The proposed material has two Dirac points in the Brillouin zone, which are protected by the mirror symmetry $\hat{M}_y$. Considering the spin–orbit coupling effect, the system turns to be non-trivial topological material. These results provide theoretical enlightenment for understanding the symmetric protecting mechanism in low-symmetry configurations, and will promote design and research on other 2D topological materials.

Keywords Dirac semimetal · two-dimensional · topological material

Introduction

Semi-metal (SM) materials,[1–4] such as Dirac semi-metal, Weyl semi-metal, and nodal line semi-metal, which have conspicuous gapless crossing points or lines near the Fermi level of the band structures, have received increasing attention for their significant physical mechanism[5,6] and potential application in nanoscale devices.[7,8] With the successful preparation in the laboratory of two-dimensional (2D) material, such as graphene,[9] silicene,[10] graphynes,[11] and some transition metal borides,[12–14] 2D Dirac semi-metal (DSM) materials[15–18] showed greater advantages than their three-dimensional (3D) counter-parts for their atomic-scale layer thickness and larger specific surface area. Combined with other important physical properties, such as magnetic,[19–22]

ferroelasticity,[23] and valleytronics,[24] research on 2D SM materials has driven the development of the next generation of low-energy transistors and electronic devices, and accelerated the progress of information technology advancement.[25–27]

Dirac points are protected by a certain structural symmetry, which is the key role for the study of DSMs. As a result, most studies have focused mainly on the materials with good symmetry, especially those with multiple symmetric protecting mechanisms.[20,28] However, the existence of Dirac points in low-symmetric configurations still lacks research. In this kind of materials, Dirac points are protected by the only symmetric operation of the configuration, which is easier to understand and modulate. By preserving and breaking the structural symmetry, the transitions between DSMs, topological insulators, and trivial materials can be realized.

In this paper, we propose a B_5ScNi monolayer as a 2D SM candidate using first-principles calculations based on density functional theory (DFT). The results of a cohesive energy and long-time molecular dynamic (MD) simulation showed a strong binding interaction and good thermodynamic stability at room temperature. Two Dirac points were observed in the Brillouin zone (BZ), protected by the only mirror symmetry of the configuration. Considering the spin–orbit coupling (SOC) effect, the non-trivial topological properties of the system have been demonstrated.

✉ Wen-Juan Li
  liwen19842003@163.com

✉ Wei-Xiao Ji
  sps_jiwx@ujn.edu.cn

1   College of Elementary Education, Changsha Normal University, Changsha 410100, People's Republic of China

2   Hunan Academy of Education Sciences, Changsha 410005, People's Republic of China

3   Spintronics Institute, University of Jinan, Jinan 250022, People's Republic of China

Computational Details

The calculations were performed by first-principles based on spin-polarized DFT using the Vienna Ab initio Simulation Package,[29–32] choosing the suffix-plus-wave projector augmented wave[33,34] pseudopotential and using the Perdew–Burke–Ernzerhof[35] approximation to describe the exchange–correlation generalized functional. The DFT + U correction[36] was applied to represent the strong correlation of electrons on the d-orbital in transition metal atoms, with $U = 2.9$ eV and 5.1 eV for Sc and Ni, respectively. The convergence of the electronic self-consist calculation was set to be less than 10^{-8} eV. To avoid the interaction between adjacent supercells, a vacuum layer larger than 20 Å was included and the plane wave truncation energy was set to 400 eV. Gaussian-type smearing of 10 meV was used on a k-point mesh of 15×23 centered around Γ for the integrations in the BZ. The atomic coordinates and the cell volume were fully optimized until the residual Hellmann–Feynman forces on each atom were smaller than 0.001 eV/Å. The SOC effect was included self-consistently. The maximum localized Wannier functions method, implemented by the WANNIER90 package,[37] was used to reconstruct the energy bands close to the Fermi energy, and the iterative Green's function[38,39] was used to calculate the density of edge states.

Results and Discussion

The fully optimized B$_5$ScNi monolayer, as shown in Fig. 1a and b, has a rectangle lattice and a nearly planar configuration with C_s structural symmetry belonging to the Pm space group (No. 6). The symmetry of B$_5$ScNi is much lower than those of other common 2D DSM materials, with only one mirror plane symmetric operator $\hat{M}_y$. The nickel (Ni) atom localizes in the same plane of the nearby boron (B) atoms, while the scandium (Sc) atom stands out of the B skeleton for about 1.02 Å along direction c. The optimized lattice constants are $a = 6.035$ Å and $b = 3.762$ Å, respectively, which was further confirmed by scanning the energy as a function of the lattice constants. The result of biaxial strain as shown in Fig. 1c, in which $\varepsilon = (a - a_0)/a_0$, a, and a_0 denote the biaxial strain and the lattice constant with and without the strain applied, respectively, and it indicates that the optimized lattice constants are indeed at the minimum in energy. The total elastic moduli are calculated to be $C_{11} = 768.3536$, $C_{22} = 493.4744$, $C_{12} = 76.6044$, and $C_{44} = 159.5674$ (all in kBar), which demonstrate the mechanical stability of B$_5$ScNi according to the Born–Huang criteria for stability ($C_{11}, C_{22}, C_{44} > 0$, and $C_{11}C_{22} - C_{12}^2 > 0$). In order to validate the thermodynamical stability of B$_5$ScNi, a long-time ab initio molecular dynamics Nosé–Hoover heat-bath simulation
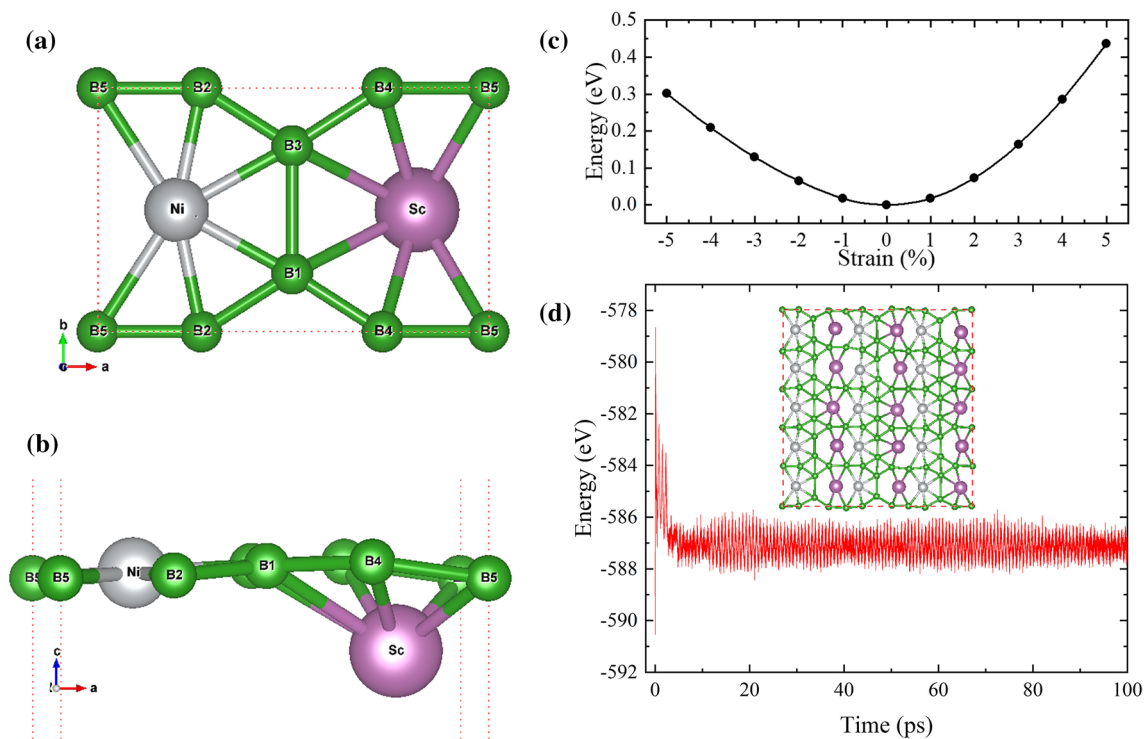

Fig. 1 (a) Top and (b) side view of the geometric structure of Born–Huang's criteriaB$_5$ScNi monolayer; (c) the energy as a function of biaxial strains; (d) the evolution of energy during the MD simulation, and the configuration at the end of the simulation (100 ps).

using a 3×5 supercell was performed at 300 K for up to 100 ps with a time step of 1 fs, and the results are plotted in Fig. 1d. Clearly, there has been no structural failure, which indicates the thermal stability of the predicted 2D B₅ScNi monolayer at room temperature.

Next, we investigated the electronic properties of Born–Huang's criteriaB₅ScNi monolayer by spin-polarized DFT calculations, and found that it has a nonmagnetic ground state. The band structure is plotted in Fig. 2a, from which it can be seen that the valence and conduction bands near the Fermi level cross each other, and the crossing point

is located at point D (0.1, 0.5, 0.0) along R–Y. Although one of the crossing bands looks nearly flat, the Dirac point D is still of type I[40]. The Fermi velocity $\hbar v_F = \mathrm{d}E(k)/\mathrm{d}k$ at the Dirac point is 1.460×10^5 m/s along D–R (comparable with graphene $\sim 8.2 \times 10^5$ m/s[41]), and 2.450×10^4 m/s along D–Y. The effective mass of the electrons is close to zero, indicating the characteristic of zero-mass Dirac fermions. Furthermore, Fig. 2b illustrates the distribution of Dirac points in the whole BZ, and two Dirac points (D and D') both located at the edge of the BZ can be observed. Figure 3a shows the orbital-projected band structure, illustrating
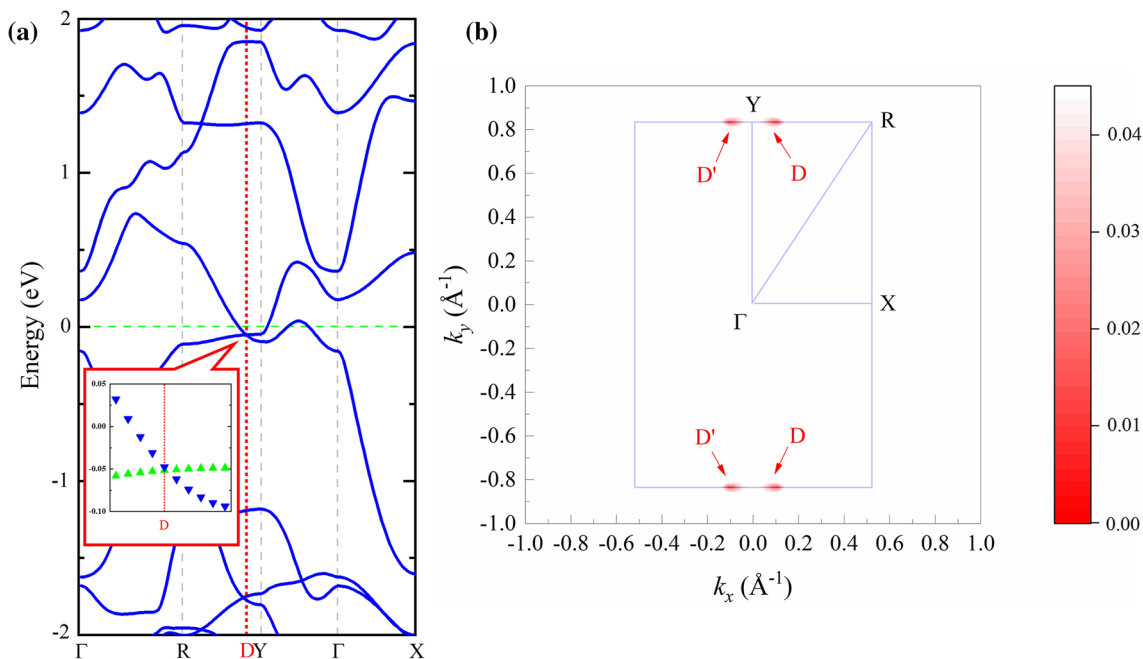
Fig. 2 (a) Band structure;(b) distribution of the two gapless Dirac points (D and D') in the first Brillouin zone, as shown in the red area (Color figure online).
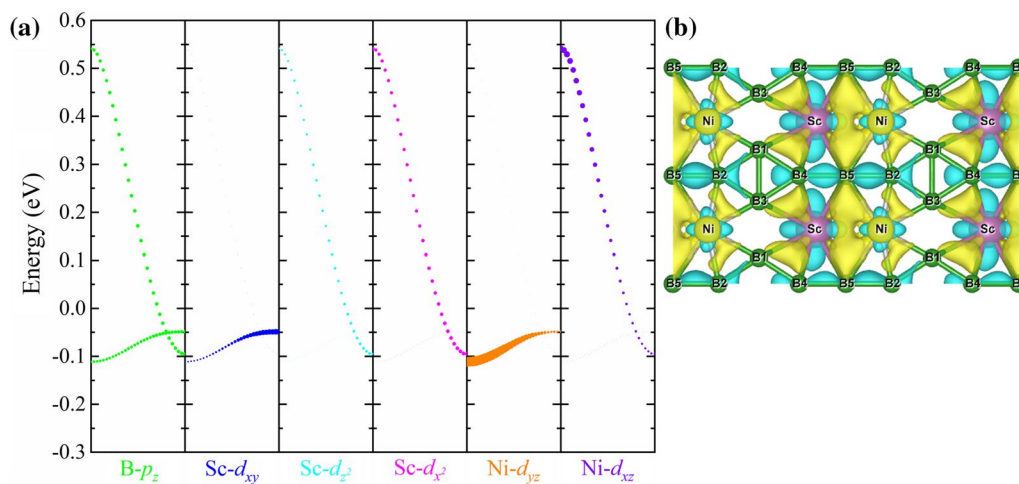
Fig. 3 (a) Orbital-resolved band structure near the Dirac point D; (b) the charge differential density of the B₅ScNi monolayer.

that the crossing bands are mainly contributed by the p_z orbitals of B and the d orbitals of Sc/Ni atoms.

To understand the bonding mechanism between the B and Sc/Ni atoms, the charge differential density was performed, which is defined as

$$\Delta\rho = \rho_{B_5ScNi} - \rho_{B_5} - \rho_{Sc} - \rho_{Ni},$$

in which ρ_{B_5ScNi} is the total charge density of B_5ScNi, ρ_{B_5} is the charge density of the B skeleton, and $\rho_{Sc(Ni)}$ is the charge density of Sc (Ni) at the free atomic state. The result is plotted in Fig. 3b, from which it can be seen that the electrons transfer mainly from the B skeleton to Sc (Ni), forming an accumulation area of electrons near the transition metal atoms. The cohesive energy, defined as

$$E_{coh} = (5E_B + E_{Sc} + E_{Ni} - E_{B_5ScNi})/7,$$

in which E_{B_5ScNi} and $E_{B(Sc,Ni)}$ are the energy of the B_5ScNi and B (Sc, Ni) atoms, is calculated to be 3.5827 eV/atom, which is higher that of Cd_4C_2 reported previously[42] (2.46 eV/atom), and indicates the strong binding strength between the atoms.

Since the Dirac point is protected by a certain structural symmetry, the analysis on the real part of the Kohn–Sham wavefunction near the crossing point was further performed to understand the protection mechanism, as shown in Fig. 4a. As mentioned above, the only symmetry in the system is the vertical mirror $\hat{M}_y$, and the chirality of real-space wave functions for the mirror was carefully checked. Obviously, the two crossing bands have opposite mirror eigenvalues ($\pm I$), so that they are orthogonal mutually with any orbital

hybridization forbidden by the mirror symmetry, resulting in the inevitable gapless Dirac point. As the Dirac points locate at the edge of the BZ, we further calculated the band structure of the 2×2 supercell to fold them inside the BZ. As shown in Fig. 4b, the Dirac point is preserved but locates along Γ–X instead, which is still clearly protected by the vertical mirror $\hat{M}_y$.

All the results above are discussed without considering the SOC effect. When the SOC effect is included, the bands with spin-up and spin-down split, and the Dirac point D is slightly gapped, as shown in Fig. 5a. The band gap induced by the SOC implies the possibility of non-trivial topological properties, and the calculation of the local density of states for the semi-infinity ribbon was performed, as shown in Fig. 5b. It can be seen that there are two edge states connecting the conduction and valence band of the bulk, indicating the existence of topological edge states.

Conclusions

We have studied the geometric and electronic band structure of a 2D semi-metal called the B_5ScNi monolayer. Our calculations show some interesting results: (1) B_5ScNi has excellent thermodynamic stability at room temperature, (2) it has two Dirac points in the BZ protected by the mirror symmetry $\hat{M}_y$, which is the only symmetry operation of the system, and (3), with the SOC considered, the Dirac points split slightly with non-trivial topological edge states. These results not only help us to under the structural protecting mechanism for configures with lower symmetry but also promote the
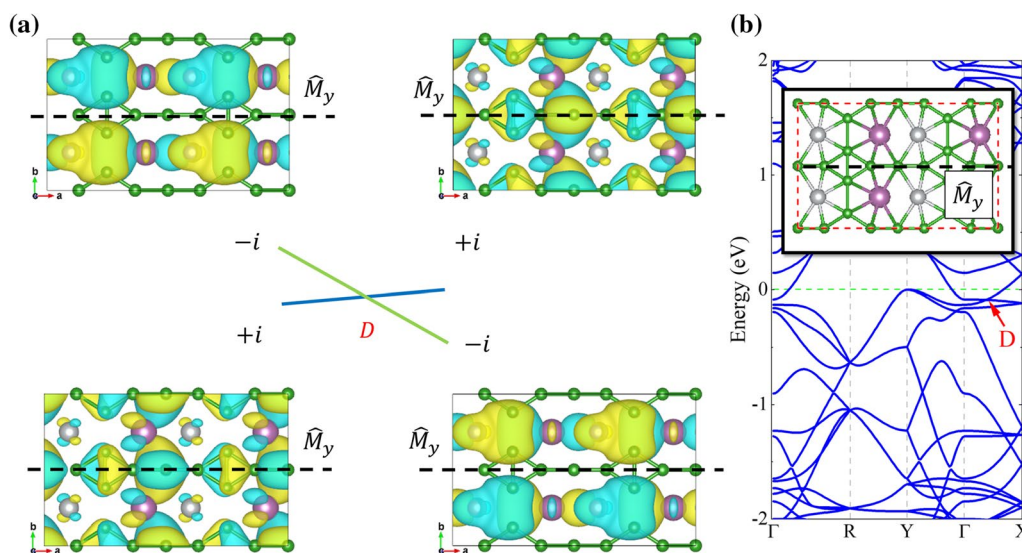
Fig. 4 (a) Wave functions close to the Dirac point D, with their Eigen values of mirror symmetry; yellow and green areas show the positive and negative values of the real part of Kohn–Sham wavefunction, respectively; (b) band structure of the 2×2 super cell, with the mirror symmetry illustrated (Color figure online).
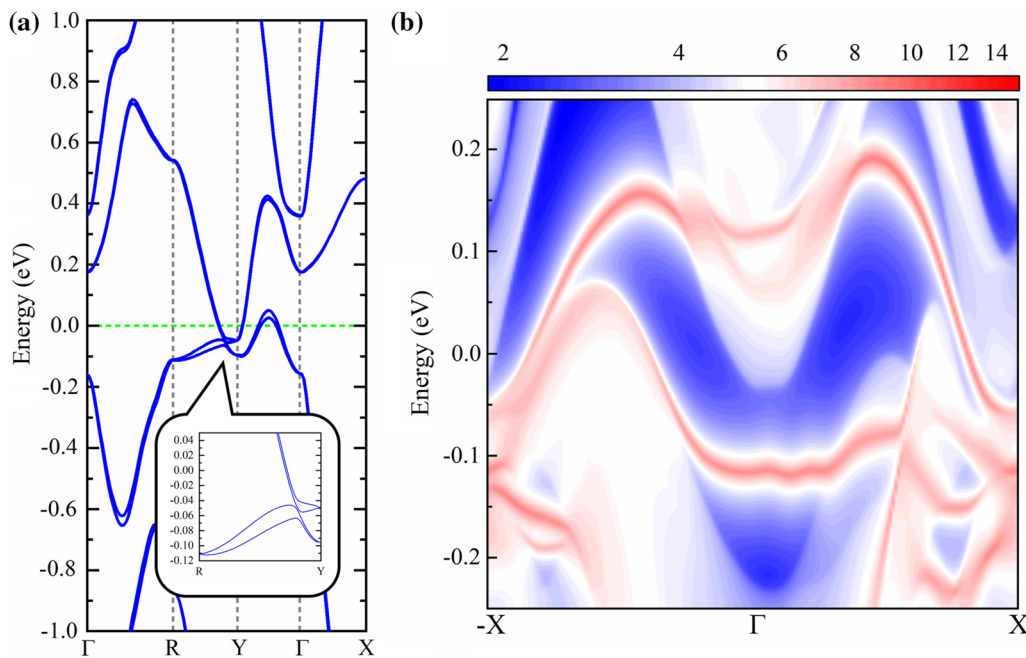
Fig. 5 (a) Band structure with SOC considered; (b) local density of the edge states, color in scale of $\log_{10}$ (Color figure online).

application of 2D semi-metal materials in nanoscale electronic devices.

Conflict of interest The authors declare that they have no conflict of interest.

References

1. K.K. Gomes, W. Mar, W. Ko, F. Guinea, and H.C. Manoharan, Designer Dirac fermions and topological phases in molecular graphene. *Nature* 483, 306 (2012).

2. S.M. Young, S. Zaheer, J.C.Y. Teo, C.L. Kane, E.J. Mele, and A.M. Rappe, Dirac semimetal in three dimensions. *Phys. Rev. Lett.* 108(14), 140405 (2012).

3. Q. Liu and A. Zunger, Predicted realization of cubic Dirac fermion in quasi-one-dimensional transition-metal monochalcogenides. *Phys. Rev. X* 7(2), 021019 (2017).

4. S.M. Young and B.J. Wieder, Filling-enforced magnetic Dirac semimetals in two dimensions. *Phys. Rev. Lett.* 118(18), 186401 (2017).

5. X.P. Yang, Y. Zhong, S. Mardanya, T.A. Cochran, R. Chapai, A. Mine, J. Zhang, J. Sánchez-Barriga, Z.-J. Cheng, O.J. Clark, J.-X. Yin, J. Blawat, G. Cheng, I. Belopolski, T. Nagashima, S. Najafzadeh, S. Gao, N. Yao, A. Bansil, R. Jin, T.-R. Chang, S. Shin, K. Okazaki, and M.Z. Hasan, Coexistence of bulk-nodal and surface-nodeless cooper pairings in a superconducting Dirac semimetal. *Phys. Rev. Lett.* 130(4), 046402 (2023).

6. J. Zhang, T.D.P. Sohier, M. Casula, Z. Chen, J. Caillaux, E. Papalazarou, L. Perfetti, L. Petaccia, A. Bendounan, A. Taleb-Ibrahimi, D. Santos-Cottin, Y. Klein, A. Gauzzi, and M. Marsi, Manipulating Dirac states in BaNiS₂ by surface charge doping. *Nano Lett.* (2023). https://doi.org/10.1021/acs.nanolett.2c04701.

7. H. Zhang, J. Huang, M. Tian, M. Liu, and Y. Zhang, 3-bit switchable terahertz coding metasurface based on Dirac semimetals. *Opt. Commun.* 527, 128958 (2023).

8. L. Cheng, Y. Xiong, L. Kang, Y. Gao, Q. Chang, M. Chen, J. Qi, H. Yang, Z. Liu, J. C. W. Song, and E. E. M. Chia, Giant photon momentum locked THz emission in a centrosymmetric Dirac semimetal. *Sci. Adv.* 9(1), eadd7856 (2023).

9. K.S. Novoselov, A.K. Geim, S.V. Morozov, D. Jiang, Y. Zhang, S.V. Dubonos, I.V. Grigorieva, and A.A. Firsov, Electric field effect in atomically thin carbon films. *Science* 306(5696), 666 (2004).

10. B. Aufray, A. Kara, S. Vizzini, H. Oughaddou, C. Leandri, B. Ealet, and G. Le Lay, Graphene-like silicon nanoribbons on Ag(110): a possible formation of silicene. *Appl. Phys. Lett.* 96(18), 183102 (2010).

11. D. Malko, C. Neiss, F. Vines, and A. Görling, Competition for graphene: graphynes with direction-dependent Dirac cones. *Phys. Rev. Lett.* 108(8), 086804 (2012).

12. Z. Gao, Q. Wang, W. Wu, Z. Tian, Y. Liu, F. Ma, Y. Jiao, and S.A. Yang, Monolayer RhB4: half-auxeticity and almost ideal spin–orbit Dirac point semimetal. *Phys. Rev. B* 104(24), 245423 (2021).

13. Y. Wang, X. Jiang, Y. Wang, and J. Zhao, Ferromagnetic Dirac half-metallicity in transition metal embedded honeycomb borophene. *Phys. Chem. Chem. Phys.* 23(32), 17150 (2021).

14. Q. Xia, Y. Hu, Y.-P. Wang, C.-W. Zhang, M.-J. Ren, S.-S. Li, and W.-X. Ji, Anisotropic nodal loop in NiB₂ monolayer with nonsymmorphic configuration. *Nanoscale* 14(4), 1264 (2022).

15. J. Wang, S. Deng, Z. Liu, and Z. Liu, The rare two-dimensional materials with Dirac cones. *Natl. Sci. Rev.* 2(1), 22 (2015).

16. S.M. Young and C.L. Kane, Dirac semimetals in two dimensions. *Phys. Rev. Lett.* 115(12), 126803 (2015).

17. W. Yi, X. Jiang, Z. Wang, T. Yang, B. Yang, and X. Liu, ABX₆ monolayers: a new Dirac material family containing high Fermi velocities and topological properties. *Appl. Surf. Sci.* 570, 151237 (2021).

18. X. Jiang, T. Yang, G. Fei, W. Yi, and X. Liu, Novel two-dimensional ABX_3 Dirac materials: achieving a high-speed strain sensor via a self-doping effect. *J. Phys. Chem. Lett.* 13(2), 676 (2022).

19. W.-X. Ji, B.-M. Zhang, S.-F. Zhang, C.-W. Zhang, M. Ding, P. Li, and P.-J. Wang, A planar C_3Ca_2 film: a novel 2p Dirac half metal. *J. Mater. Chem. C* 5(33), 8504 (2017).

20. W.-X. Ji, B.-M. Zhang, S.-F. Zhang, C.-W. Zhang, M. Ding, P.-J. Wang, and R. Zhang, Na_2C monolayer: a novel 2p Dirac half-metal with multiple symmetry-protected Dirac cones. *Nanoscale* 10(28), 13645 (2018).

21. G.-G. Li, R.-R. Xie, L.-J. Ding, W.-X. Ji, S.-S. Li, C.-W. Zhang, P. Li, and P.-J. Wang, Two-dimensional Weyl semi-half-metallic $NiCS_3$ with a band structure controllable by the direction of magnetization. *Phys. Chem. Chem. Phys.* 23(21), 12068 (2021).

22. Z. Liu, J. Liu, and J. Zhao, YN_2 monolayer: Novel p-state Dirac half metal for high-speed spintronics. *Nano Res.* 10(6), 1972 (2017).

23. X. Ding, Y. Ge, Y. Jia, G. Gou, Z. Zhu, and X.C. Zeng, InBi: a ferroelastic monolayer with strain tunable spin-orbit dirac points and carrier self-doping effect. *ACS Nano* 16(12), 21546 (2022).

24. Z. Liu, W. Feng, H. Xin, Y. Gao, P. Liu, Y. Yao, H. Weng, and J. Zhao, Two-dimensional spin–valley-coupled Dirac semimetals in functionalized SbAs monolayers. *Mater. Horiz.* 6(4), 781–787 (2019).

25. K.S. Novoselov, A.K. Geim, S.V. Morozov, D. Jiang, M.I. Katsnelson, I.V. Grigorieva, S.V. Dubonos, and A.A. Firsov, Two-dimensional gas of massless Dirac fermions in graphene. *Nature* 438(7065), 197 (2005).

26. A.K. Geim and K.S. Novoselov, The rise of graphene. *Nat. Mater.* 6(3), 183 (2007).

27. S.V. Morozov, K.S. Novoselov, M.I. Katsnelson, F. Schedin, D.C. Elias, J.A. Jaszczak, and A.K. Geim, Giant intrinsic carrier mobilities in graphene and its bilayer. *Phys. Rev. Lett.* 100(1), 016602 (2008).

28. Z. Lv, N. Jia, J. Cai, X. Jiang, J. Zhao, and Z. Liu, Mechanical anisotropy and multiple direction-dependent Dirac states in a synthesized Ag_3C_{20} monolayer. *Phys. Rev. B* 106(19), 195429 (2022).

29. G. Kresse and J. Furthmuller, Efficiency of ab-initio total energy calculations for metals and semiconductors using a plane-wave basis set. *Comput. Mater. Sci.* 6(1), 15 (1996).

30. G. Kresse and J. Furthmuller, Efficient iterative schemes for ab initio total-energy calculations using a plane-wave basis set. *Phys. Rev. B* 54(16), 11169 (1996).

31. G. Kresse and J. Hafner, Ab initio molecular dynamics for liquid metals. *Phys. Rev. B* 47(1), 558 (1993).

32. G. Kresse and J. Hafner, Ab initio molecular-dynamics simulation of the liquid-metal amorphous-semiconductor transition in germanium. *Phys. Rev. B* 49(20), 14251 (1994).

33. P.E. Blochl, Projector augmented-wave method. *Phys. Rev. B* 50(24), 17953 (1994).

34. G. Kresse and D. Joubert, From ultrasoft pseudopotentials to the projector augmented-wave method. *Phys. Rev. B* 59(3), 1758 (1999).

35. J.P. Perdew, K. Burke, and M. Ernzerhof, Generalized gradient approximation made simple. *Phys. Rev. Lett.* 77(18), 3865 (1996).

36. S.L. Dudarev, G.A. Botton, S.Y. Savrasov, C.J. Humphreys, and A.P. Sutton, Electron-energy-loss spectra and the structural stability of nickel oxide: an LSDA+U study. *Phys. Rev. B* 57(3), 1505 (1998).

37. A.A. Mostofi, J.R. Yates, Y.-S. Lee, I. Souza, D. Vanderbilt, and N. Marzari, Wannier90: a tool for obtaining maximally-localised Wannier functions. *Comput. Phys. Commun.* 178(9), 685 (2008).

38. M.P. Lopez Sancho, J.M. Lopez Sancho, and J. Rubio, Quick iterative scheme for the calculation of transfer matrices: application to Mo (100). *J. Phys. F Metal Phys.* 14(5), 1205 (1984).

39. M.P. Lopez Sancho, J.M. Lopez Sancho, J.M.L. Sancho, and J. Rubio, Highly convergent schemes for the calculation of bulk and surface Green functions. *J. Phys. F Metal Phys.* 15(4), 851 (1985).

40. H. Huang, S. Zhou, and W. Duan, Type-II Dirac fermions in the $PtSe_2$ class of transition metal dichalcogenides. *Phys. Rev. B* 94(12), 121117 (2016).

41. D. Malko, C. Neiss, F. Viñes, and A. Görling, Competition for graphene: graphynes with direction-dependent Dirac cones. *Phys. Rev. Lett.* 108(8), 086804 (2012).

42. L.B. Meng, S. Ni, Y.J. Zhang, B. Li, X.W. Zhou, and W.D. Wu, Two-dimensional zigzag-shaped Cd_2C monolayer with a desirable bandgap and high carrier mobility. *J. Mater. Chem. C* 6(34), 9175 (2018).